Catalytic Mechanism of Hydroxynitrile Lyase from *Hevea brasiliensis*: A Theoretical Investigation

Feng-Chao Cui, Xiao-Liang Pan, and Jing-Yao Liu*

State Key Laboratory of Theoretical and Computational Chemistry, Institute of Theoretical Chemistry, Jilin University, Changchun 130023, China

Received: January 14, 2010; Revised Manuscript Received: May 7, 2010

Density functional theory (DFT) calculations using the hybrid functional B3LYP have been performed to investigate the catalytic mechanism of hydroxynitrile lyase from *Hevea brasiliensis* (Hb-HNL). This enzyme catalyzes the cleavage of acetone cyanohydrin to hydrocyanic acid plus acetone. Two models (A and B) of the active site consisting of 105 and 155 atoms, respectively, were constructed on the basis of the crystal structure. Good consistency between the two models provides a verification of the proposed mechanism. Our calculations show that the catalytic reaction proceeds via three elementary steps: (1) deprotonation of the OH-Ser80 by His235 and concomitant abstraction of a proton from the substrate hydroxyl by Ser80; (2) the C−C bond cleavage of the acetone cyanohydrin; and (3) protonation of the cleaved cyanide by His235. The cleavage of the C−C bond is the rate-limiting step with the overall free energy barrier of 13.5 kcal/mol for relatively smaller model A (14.9 kcal/mol for a larger model B) in the protein environment, which is in good agreement with experimental rate. The present results give support to the previously proposed general acid/base catalytic mechanism, in which the catalytic triad acts as a general acid/base. Moreover, the calculated results for model C, with the positive charge of Lys236 removed from model A, show that Lys236 with the positive charge plays a vital role in lowering the reaction barrier of the rate-determining and helps in stabilizing the negatively charged CN^- by forming a hydrogen bond with the substrate, consistent with the experimental analysis.

1. Introduction

Hydroxynitrile lyases, HNLs(EC 4. 1. 2. 39), are important enzymes for the catabolism of cyanogenic glycosides during cyanogenesis[1] and the metabolism of these compounds during seedling development[2,3] in several species of cyanogenic plants.[1,4] HNLs can catalyze the cleavage of cyanohydrins into hydrocyanic acid (HCN) and the corresponding aldehyde or ketone, as shown in Figure 1.[5] The liberated HCN not only plays a significant defensive role in plant system against herbivores and microbial attack[5−7] but also serves as a nitrogen source for the biosynthesis of L-asparagine.[8,9] In addition, by employing the reversible enzymatic reaction, HNLs are used as versatile biocatalysts for the enantioselective synthesis of chiral cyanohydrins,[10−14] which are important synthetic intermediates in the fields of fine chemicals, pharmaceuticals, and agrochemicals. Therefore, as important enzymes and biocatalysts, HNLs have attracted considerable biologists' and chemists' attentions over the past years.[15−18]

The present work focuses on the HNL from the tropical rubber tree *Hevea brasiliensis* (Hb-HNL), which belongs to the α/β-hydrolases superfamily[19−21] based on crystallographic structure analysis.[19] Its biological substrate is the achiral acetone cyanohydrin.[22,23] Similar to other hydrolases, the active site of the Hb-HNL contains a conserved catalytic triad, consisting of three amino residues Ser80, His235, and Asp207. In more than 10 years, two catalytic mechanistic schemes have been proposed for the Hb-HNL. One supposed that the catalytic process of Hb-HNL resembles the widely accepted serine hydrolases mechanism,[19,24] which involves a hemiacetal or hemiketal covalently bound intermediate resulting from nucleophilic attack of the active site serine on the substrate. However, the subsequent structural studies on Hb-HNL−inhibitor complexes[25] as well as modeling studies[26] did not give support to this hypothesis. Instead, on the basis of the structure data, an alternative reaction mechanism was put forward that the conserved catalytic triad acts as a general acid/base[18,25,26] rather than a nucleophile.[19] As shown in Figure 2, it was suggested that the reaction proceeds via a double-proton transfer process, that is, the deprotonation of the substrate by Ser80, which in turn is deprotonated by His235, followed by C−C bond cleavage of the substrate leading to the formation of ketone and cyanide ion (CN^-); then, His235 reprotonates the cyanide ion to form HCN.[18,25] Lys236 was also suggested to play an important role in stabilizing the nascent cyanide CN^- in the catalytic process.[18] Although the experimental data seemed to give a reasonable description for the acid/base catalytic mechanism of Hb-HNL, exactly how these steps occur is still unclear; for example, it still remains controversial whether the deprotonation and the C−C cleavage of the substrate takes place concerted or stepwise.

Theoretically, only one ab initio study for the protonation states in the enzyme active site of Hb-HNL was reported.[17] To the best of our knowledge, few theoretical studies on the mechanism have been addressed. To examine the feasibility of the suggested mechanism and give a detailed description of each

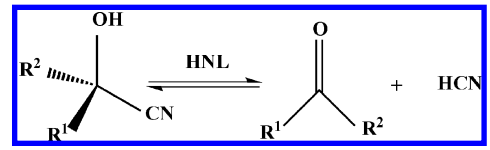

Figure 1. Reaction catalyzed by hydroxynitrile lyases.

* To whom correspondence should be addressed. E-mail: ljy121@jlu.edu.cn.

10.1021/jp100373e
Published on Web 07/01/2010

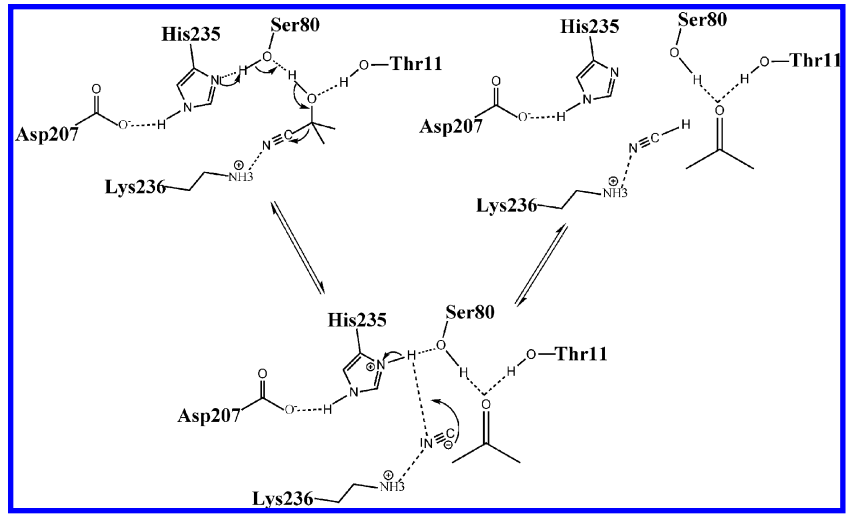

Figure 2. Proposed mechanism of the reaction catalyzed by Hb-HNL formulated for the cyanohydrin cleavage direction.[18,25]

individual step, we have investigated the process of Hb-HNL-catalyzed cyanohydrin cleavage by density functional theory (DFT) calculations. Here the B3LYP functional of DFT, which has been widely accepted as a powerful tool for analyzing the catalytic mechanism of enzyme,[27−35] is employed to evaluate the energetics and to understand the mechanism. The rest of the apoenzyme environment is treated as a dielectric continuum solvation model.

2. Computational Details

In the present study, quantum chemistry calculations were performed using the DFT with Becke's three-parameter (B3)[36] exchange functional along with the Lee−Yang−Parr (LYP)[37,38] nonlocal correlation functional (B3LYP). The geometries were optimized by using the 6-31g(d,p) basis set. Some centers were fixed to preserve the positions of the active site residues as similar as those in the crystal structure during the optimization. To obtain more accurate energetics, single-point calculations were done at the same level but with larger basis set 6-311+G(2d,2p) on the B3LYP/6-31G(d,p) optimized geometries. Frequency calculations have been done at the B3LYP/6-31G(d,p) level to characterize the nature of the stationary points, that is, the minima with all real frequencies and the transition states with only one imaginary frequency, and to obtain the thermal corrections to Gibbs free energy at 298 K. As is well-known, the free energy change is comprehensively used to characterize the reactions for such enzymatic systems. For each transition state, intrinsic reaction coordinate (IRC) calculations were performed to guarantee its correct connection to the designated local minima. Natural population atomic (NPA) charges were determined with the natural bond orbital (NBO) analysis[39−41] at the same level. To evaluate solvation effects of the missing protein environment, the Gibbs free energy of solvation for each species was calculated by using the integral equation formalism polarizable continuum model (IEF-PCM)[42−44] based on B3LYP/6-31G(d,p) optimized structures in the gas phase. The effects of the surrounding active site were represented by polarizable dielectric continuum. The dielectric constant was set to four, which is the standard value used to model protein surrounding.[45] The free energy of each species in solution is taken as the sum of the gas-phase free energy (the B3LYP/6-311+G(2d,2p) single-point energy with inclusion of B3LYP/6-31G(d,p) thermal correction) and the free energy of solvation. All computations were performed by using the Gaussian03 package of programs.

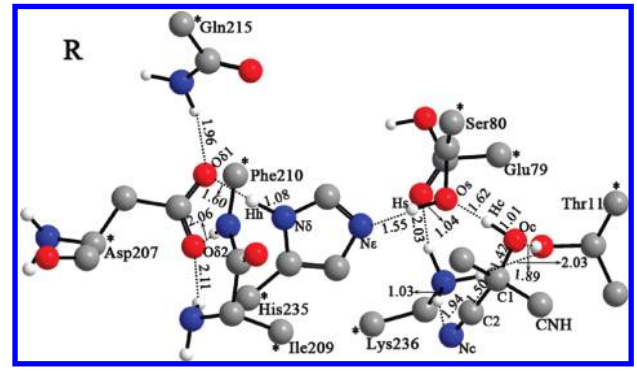

Figure 3. Optimized structure of the Hb-HNL active site model complex with the acetone cyanohydrin. Some hydrogen atoms are omitted for clarity. Atomic distances are in angstroms. Asterisks indicate the atoms fixed in their X-ray positions in the calculations.

3. Active-Site Model

The model of the Hb-HNL active site is constructed on the basis of the X-ray crystal structure of the enzyme complex with the acetone cyanohydrin (PDB entry 1SC9).[18] We consider only the residues that are directly involved in the reaction and in correctly positioning the substrate and reactive residues. The model (called A) consists of 105 atoms, and the following groups are included (Figure 3): (1) three residues of the catalytic triad (Asp207-His235-Ser80), where Asp207 is represented by the whole side chain and part of backbone of Asp207 residue, and His235 and Ser80 are represented by methyl imidazole ring and ethanol, respectively; (2) $C\beta$ of side chain, the $C\alpha$ and α amino group of Ile209, and the part of backbone between Ile209 and Phe210 (C−N−$C\alpha$) as the α amino groups of Ile209 and Phe210 make hydrogen bonds to the carboxyl Oδ2 of Asp207; (3) amide side chain of Gln215 because this group forms hydrogen bond to Oδ1 of Asp207; (4) Lys236 and Thr11, because they are important to bind and orientate the substrate, are represented by ethyl ammonium and 2-propanol, respectively; and (5) side chain of Glu79, modeled as an acetic acid. Note that Glu79 is protonated in this model. There are two reasons for this treatment of Glu79: First, when the deprotonated Glu79 is presented in this model, the anionic of Glu79 is not stabilized, and the optimization of the reactant always leads to a structure with transfer of the proton from Lys236 to Glu79 (as shown in the Supporting Information, Figure S1). Clearly, this model is not reasonable because it has been suggested in experiment by Gruber et al.[18] that Lys236 with positive charge

plays an important role in the catalytic reaction. This conclusion has also been verified by our calculations in the following section. Second, the anionic of Glu79 could be stabilized when some residues around it are included in a larger model. Apparently, to perform calculations using a larger model is much more computationally demanding. Therefore, to keep stability of the positively charged Lys236 and meanwhile consider the compromise between the computational accuracy and cost, we choose Glu79 being protonated in model A.

In addition, to validate the rationality of the mechanism proposed by model A, a larger model (called model B) is employed with the total size of 152 atoms. It contains the parts of the side chain of Trp128, His14, Cys81, and Gln238 and the backbone between His10 and Thr11 in addition to model A. In this model, Glu79 is deprotonated, and Gln238 and Thr11 form hydrogen bonds to it. Also, to investigate the role of Lys236 with positive charge for the catalytic reaction, we build another model (called model C), in which the positive charge of Lys236 is removed from model A and Glu79 is also deprotonated because of the absence of the positive charge of Lys236. The equivalent calculations for models B and C are performed at the same level as those for model A. Unless noted, the results and discussion obtained by model A are reported in the following section.

4. Results and Discussion

4.1. Double-Proton Transfer. The constrained optimized structure of the Hb-HNL active site regarded as the reactant species R is displayed in Figure 3. It is clearly observed that the hydrogen bond networks are well reproduced in the reactant similar to those in the crystal structure.[18] The substrate is hydrogen bonded to the residues Thr11, Lys236, and Ser80, with lengths of 2.86, 2.93, and 2.61 Å, respectively. (Hydrogen bond distances will here always refer to the distance between the donor and acceptor atoms.) These hydrogen bonds help in stabilizing the substrate and orienting it in a favorable position for being deprotonated by Ser80. The three residues, Ile209, Phe210, and Gln215, form hydrogen bonds to carboxyl oxygen of Asp207, with distances of 3.05, 3.07, and 2.96 Å, respectively. The hydrogen bonds are also observed between the Oδ1 atom of Asp207 and the Nδ atom of His235 and between the Os atom of Ser80 and the Nε atom of His235, and the hydrogen bond distances are calculated to be 2.67 and 2.59 Å, respectively. It is seen that the intramolecular hydrogen bonds of the catalytic triad locate the Os−H of Ser80, the imidazole ring of His235, and the Oδ1 atom of Asp207 in a nearly planar.

The optimized structures of the transition state (TS1) and intermediate (Int1) for the double-proton transfer are displayed in Figure 4. The bond distance of Oc-Hc of the substrate is gradually elongated (from 1.01 Å in R to 1.15 Å in TS1 and to 1.47 Å in Int1), and the Os-Hc bond distance is decreased (from 1.62 Å in R to 1.27 Å in TS1 and to 1.05 Å in Int1), which means that the acetone cyanohydrin has been deprotonated by Ser80. Meanwhile, the Hs atom of Ser80 is also transferred toward the Nε atom of His235, and the calculated distance of Os−Hs bond of Ser80 increases from 1.04 Å in R to 1.43 Å in TS1, and to 1.65 Å in Int1. From the distances in TS1a, one can see that the double-proton transfer is concerted but not precisely synchronous. The proton transfer from the Oc atom of the substrate to the Os atom of Ser80 is in the early stage, whereas the proton abstraction from Ser80 by His235 is in the later stage. This protonation/deprotonation process can further be confirmed by NBO analysis. The NPA charges calculated at the B3LYP/6-31 g(d,p) level are listed in Table 1. It is seen

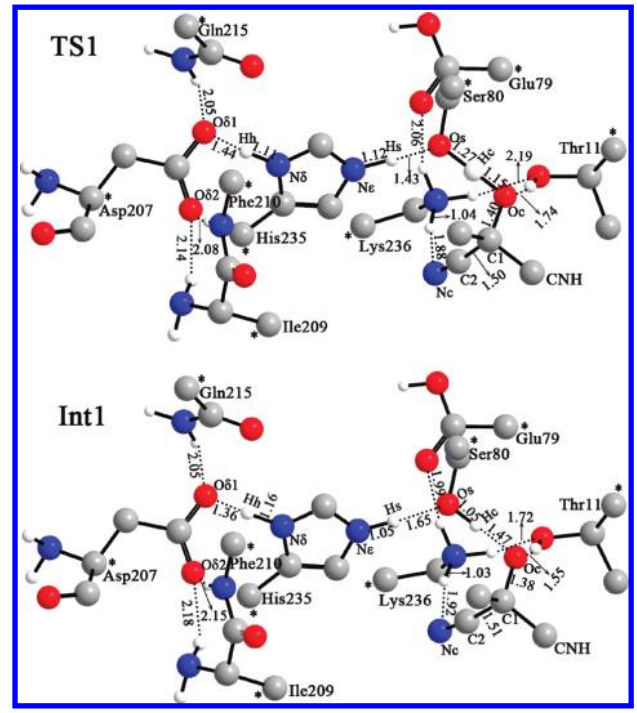

Figure 4. Optimized structures of the transition state and intermediate in the first step.

TABLE 1: Natural Population Atomic Charges in Species Involved in All Elementary Steps[a]

species	R	TS1	Int1	TS2	Int2	TS3	Int3
Os	–0.852	–0.892	–0.856	–0.826	–0.823	–0.804	–0.807
Oc	–0.796	–0.829	–0.864	–0.737	–0.649	–0.626	–0.623
Hs	0.514	0.484	0.476	0.475	0.473	0.311	0.264
Hc	0.519	0.518	0.519	0.522	0.517	0.496	0.501
C1	0.196	0.205	0.215	0.535	0.660	0.641	0.634
C2	0.353	0.372	0.359	0.117	0.039	0.054	0.079
Nc	–0.452	–0.463	–0.478	–0.696	–0.807	–0.526	–0.405
Nε	–0.611	–0.562	–0.551	–0.548	–0.548	–0.583	–0.609
Nδ	–0.545	–0.534	–0.531	–0.514	–0.530	–0.541	–0.550
Oδ1	–0.777	–0.773	–0.773	–0.772	–0.774	–0.777	–0.778

[a] Label of atoms for each species is given in Figures 3, 4, 6, and 7.

that the charge around Oc becomes more and more negative, and the charge around Nε becomes less and less negative from R to Int1, whereas the negative charge distributed on Os increases from R to TS1 and subsequently decreases in Int1. The changes of charge around Os, Nε, and Oc also illustrate that this step is a double-proton transfer process. The hydrogen bond distance between Thr11 and the substrate is gradually shortened from 2.86 Å in R to 2.72 Å in TS1 and to 2.56 Å Int1, indicating that the hydrogen bond interaction is strengthened in Int1. Consequently, Thr11 may assist in stabilizing the deprotonated substrate with more negative charge distributed on Oc atom.

Energetically, the Gibbs free energy barrier of this step at 298K in the gas phase is calculated to be 4.0 kcal/mol at the B3LYP/6-311+G(2d,2p)//B3LYP/6-31G(d,p) level, and the reaction is slightly exothermic by −1.3 kcal/mol, as shown in Figure 5. To consider the effects of the protein electrostatic environment, the single-point IEF-PCM calculations were performed at the B3LYP/6-31G(d,p) level. One can see that this step is endothermic by 1.6 kcal/mol and involves a free energy barrier of 6.9 kcal/mol when including the solvent effects.

4.2. C−C Cleavage of Acetone Cyanohydrin. The transition state (TS2) and intermediate (Int2) for C−C decomposition

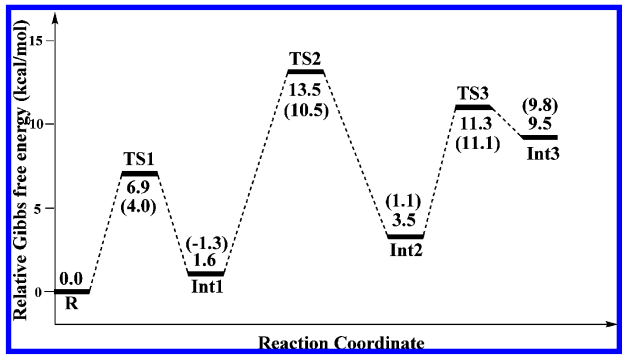

Figure 5. Computed free energy profile of the whole reaction catalyzed by Hb-HNL in the solution and in gas phase (in parentheses) by using model A. Relative energies with respect to the reactant are given in kilocalories per mole.

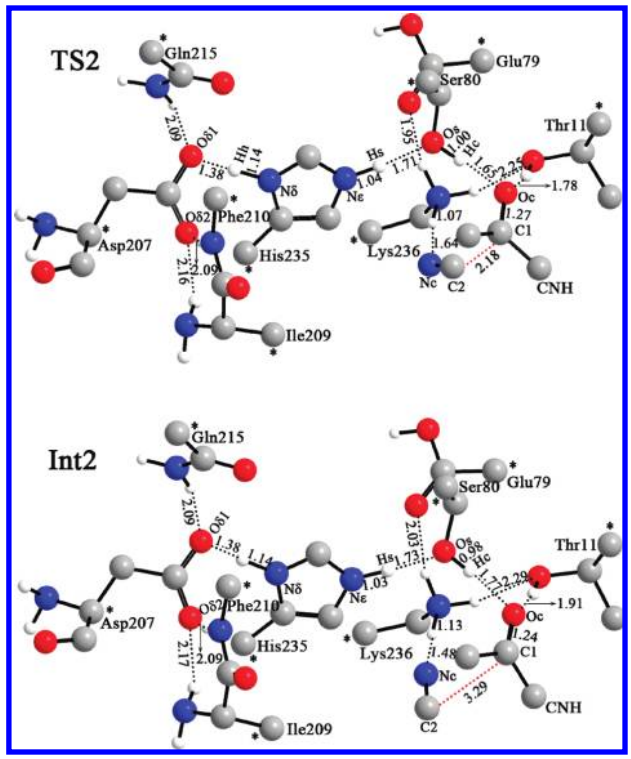

Figure 6. Optimized structures of the transition state and intermediate in the second step.

were located (Figure 6). The distance of C−C bond of the substrate increases from a single covalence bond with characteristic length of 1.51 Å in Int1 to a noncovalence bond with length of 2.18 Å in TS2 and up to 3.29 Å in Int2. Meanwhile, the C−O single bond of the substrate also becomes C═O double bond with a distance of 1.24 Å in Int2. The NPA charges on C2 and Nc are predicted to be 0.117 and −0.696 au in TS2, respectively, and 0.039 and −0.807 au in Int2. This indicates that the C−C bond is almost broken in TS2, and the negatively charged hydrocyanic (CN^-) is formed. The hydrogen-bond lengths between the acetone and Ser80 and between the acetone and Thr11 are calculated to be 2.64 and 2.75 Å in TS2, respectively, which are fairly close to the distance 2.60 and 2.80 Å in the X-ray structure of the enzyme complex with the acetone.[25] It is also observed that the hydrogen-bond lengths between Lys236 and the substrate in TS2 and Int2 become 0.23 and 0.32 Å shorter than that in R, respectively, indicating that a very strong hydrogen bond interaction exists in Int2, and as a result, the nascent negative CN^- would be stabilized by Lys236. Moreover, it should be noted that the hydrogen bond

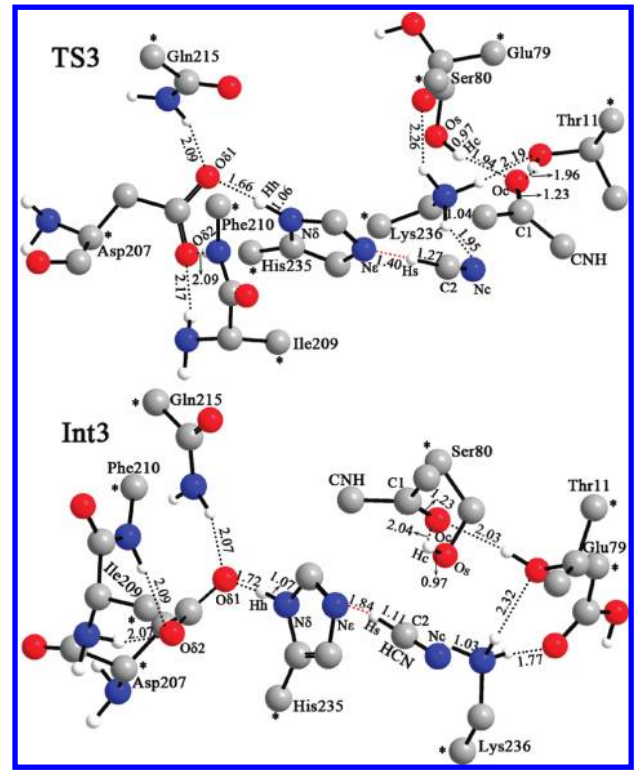

Figure 7. Optimized structures of the transition state and intermediate in the last step.

distance between Nδ of His235 and Oδ1 of Asp207 is shortened somewhat from R to Int1 (2.67, 2.55, and 2.52 Å for R, TS1, and Int1, respectively) in the initial step of the double-proton transfer, and this short distance still is maintained in the step of C−C bond cleavage. Therefore, Asp207 may play a vital role in stabilizing the protonated His235 during the reaction process. The Gibbs free energy barrier of this dissociation process is calculated to be 13.5 kcal/mol with inclusion of solvent effects by using IEF-PCM model (the relative value of 11.8 kcal/mol in gas phase), and this step is endothermic by 1.9 kcal/mol (2.4 kcal/mol in gas phase) with regard to Int1.

4.3. Protonation of Hydrocyanic (CN^-). In Figure 7, the optimized structures of the transition state (TS3) and intermediate (Int3) are displayed. The transition state, TS3, characterizes the hydrocyanic CN^- being protonated by His235. In TS3, the breaking Nε-Hs bond is stretched to 1.40 Å, and the forming Hs-C2 bond is shortened to 1.27 Å, which means that a proton is being transferred from His235 to CN^-. The changes of NPA charge on Nε, Nc, and C2 listed in Table 1 also confirm that CN^- accepts a proton from His235. We note that for His235 imidazole ring, a small rotation takes place in going from Int2 to TS3 to facilitate the proton abstraction of hydrocyanic from His235. In addition, it is found that the hydrogen-bond interaction between Lys236 and HCN in product disappears with the distance of 3.38 Å between the N atom of Lys236 and the Nc atom of HCN. This change makes the departure of HCN from the active site easier, leading to the separate final product P and HCN. The free energy barrier of this step is predicted to be 10.0 kcal/mol in the gas-phase relative to Int2 and decreases to 7.8 kcal/mol after considering the solvent effects.

To get an estimate of how important the residue Lys236 with the positive charge could be in the catalytic reaction, we perform the equivalent calculations with model C, in which the positive charge of Lys236 is removed from the active site model A. The corresponding optimized structures of the transition state (TS-

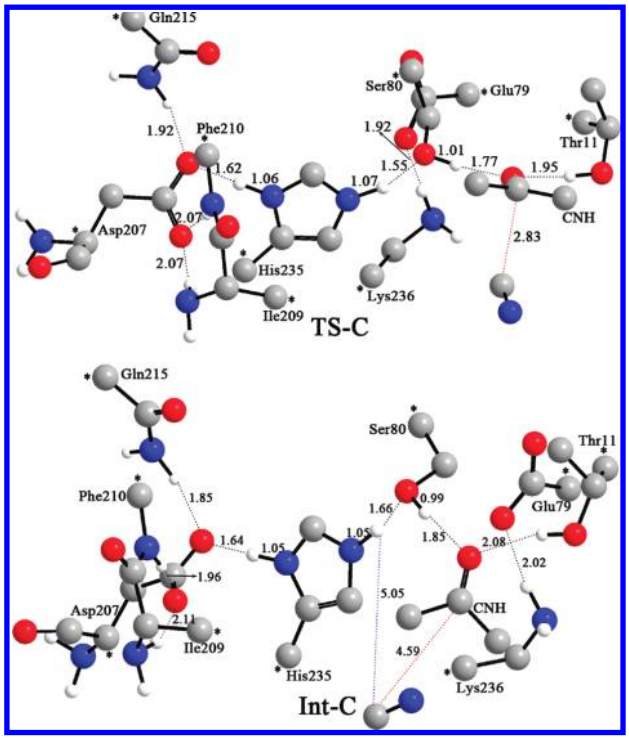

Figure 8. Optimized transition-state (TS-C) and intermediate (Int-C) structure for the model in which the positive charge of Lys236 was removed (model C).

C) and intermediate (Int-C) are shown in Figure 8. We have tried to locate the same double-proton-transfer transition state as obtained by model A in the first step of the catalytic reaction but failed. Instead, a concerted transition state of the double-proton-transfer and the C−C cleavage as shown in Figure 8 was found. The corresponding free energy barrier is 18.2 kcal/mol in the protein environment at the B3LYP/6-311+G(2d,2p)//B3LYP/6-31G(d,p) level, suggesting that the absence of the positive charge of Lys236 could increase the activation barrier of the rate-limiting step by ~4.7 kcal/mol. Also, it is observed from Figure 8 that in this case the CN^- does not form the hydrogen bond with Lys236. We have attempted to locate the transition state of CN^- protonated by His235 but without success. Consequently, one can conclude that Lys236 with positive charge plays an important role in lowering the activation barrier and stabilizing the negative CN^-.

On the basis of the calculations presented above, it is concluded that the catalytic reaction of Hb-HNL employs a general acid/base catalytic mechanism, in line with the related experimental hypothesis by Gruber et al.[18,25] It should be noted that, however, in their paper they speculated that the former two steps are likely to occur concertedly. To find this possible reaction pathway, we made many attempts to locate a concerted TS (as suggested by Gruber et al), in which proton transfer from the substrate to Ser80 coincides with the C−C bond cleavage, but without success. Therefore, we concluded that the proton transfer and the cleavage of C−C most likely occur by a stepwise mechanism rather than a concerted one. Overall, present calculations show that the catalytic reaction proceeds via a three-step mechanism: (1) double proton transfer process, which involves a proton transfer from the substrate to Ser80 and a proton transfer from Ser80 to His235; (2) C−C bond cleavage of the substrate to form the acetone and hydrocyanic anion CN^-; and (3) protonation of CN^- leading to HCN. The cleavage of the C−C bond is the rate-limiting step with an accumulated free energy barrier of 13.5 kcal/mol in the protein

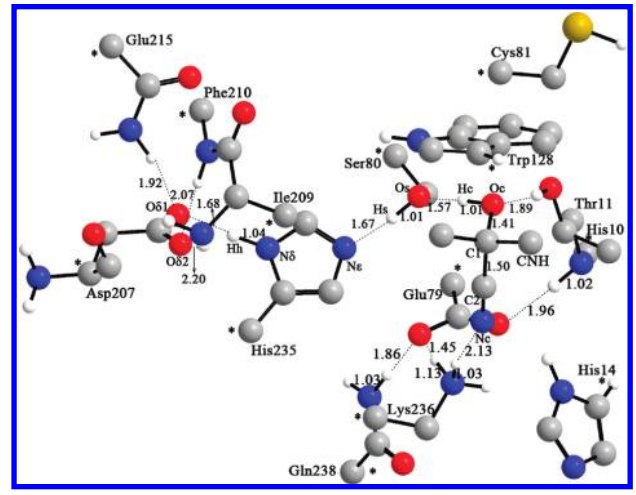

Figure 9. Optimized structure of the reactant for model B.

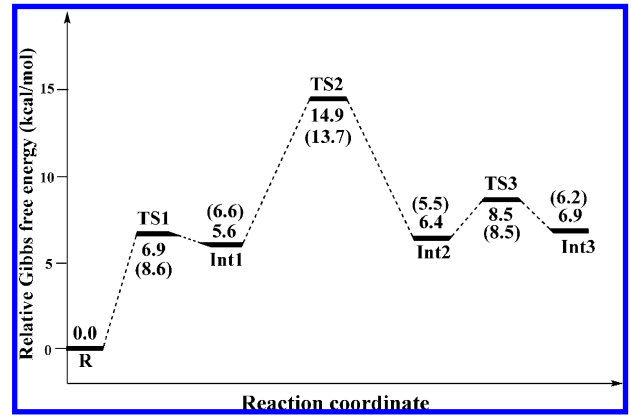

Figure 10. Computed free energy profile of the whole reaction catalyzed by Hb-HNL in the solution and in gas phase (in parentheses) by employing model B. Relative energies with respect to the reactant are given in kilocalories per mole.

environment by employing model A. Given that B3LYP method generally underestimates a few kilocalories per mole barrier heights,[46] the calculated barrier height of the rate-limiting step for model A is in reasonable agreement with the experimental value, 16.1 kcal/mol, deduced from the measured rate constant[47] (k_{cat} = 10 s^- at 298 K) by classical transition state theory. In addition, the calculated results of model C show that Lys236 with positive charge plays an important role in lowering the rate-limiting barrier and helps in stabilizing CN^- generated by making a hydrogen bond to substrate, as suggested from experiment by Gruber et al.[18]

To validate the rationality of the calculated results obtained by employing model A, the mechanismic study has also been done with a larger model (model B), which is much more computational demanding (152 atoms in model B vs 105 atoms in model A). The optimized structure of the reactant is displayed in Figure 9, and the free energy profile is shown in Figure 10. The structures of other stationary points are shown in the Supporting Information (Figures S2−S7). It can be seen that model B exhibits the same three-step reaction mechanism as described above. Also, comparing the results of the two models, one can find that the larger model B would increase the rate-limiting barrier by 1.4 kcal/mol, yielding better agreement with the experiment value. The good agreements between models A and B and between them and experiment indicate that model A could provide a proper description for this catalytic reaction, and the proposed mechanism and energies obtained in this study are reliable.

5. Conclusions

In this work, we have presented a detailed quantum mechanical study for the reaction of the catalytic cleavage of the acetone cyanohydrin by Hb-HNL. The calculations of models A and B indicate that the catalytic triad acting as a general acid/base plays an important catalytic role in the reaction, and Hb-HNL employs a general acid/base mechanism, in line with the experimental hypothesis. The reaction starts with a double proton transfer process, followed by the cleavage of the C−C bond of the substrate and then CN^- being protonated to generate the final product. This three-step mechanism is slightly different from the previously proposed two-step mechanism. The energies of all elementary reaction steps involved in the catalytic reaction were calculated at the B3LYP/6-31 g(d,p) level, and the effects of solvation were considered by the integral equation formalism polarizable continuum model (IEF-PCM). The calculated free energy profile indicates that the second step, that is, the cleavage of the C−C bond, is the rate-limiting step in the whole catalytic reaction, and the overall free energy barriers of 13.5 kcal/mol in model A and 14.9 kcal/mol in model B with consideration of the solvent effects are in good agreement with the corresponding experimental value.[47] It is seen that the solvent effects do not change the basic character of the free energy profile obtained in the gas phase, only shifting the energies of each step by a few kilocalories per mole. In addition, the calculation of model C demonstrates that Lys236 with positive charge plays an important role in lowering the activation barrier of rate-limiting step and helps in stabilizing CN^- generated by making a hydrogen bond to substrate, same as the experimental suggestion by Gruber et al.[18]

Acknowledgment. This work was supported by the National Natural Science Foundation of China (20973077), the Program for New Century Excellent Talents in University (NCET). We are grateful to the referees for their valuable comments on improving the manuscript.

Supporting Information Available: Structures of other stationary points. This material is available free of charge via the Internet at http://pubs.acs.org.

References and Notes

(1) Poulton, J. E. Localization and Catabolism of Cyanogenic Glycosides. In*Cyanide Compounds in Biology*; Evered, D., Harnett, S., Eds.; Ciba Foundation Symposium *140*; John Wiley and Sons: Chichester, U.K., 1988; pp 67−91.

(2) Selmar, D.; Lieberei, R.; Biehl, B. Mobilization and Utilization of Cyanogenic Glycosides: The Linustatin Pathway. *Plant Physiol.* **1988**, *86*, 711–716.

(3) Selmar, D.; Lieberei, R.; Biehl, B.; Conn, E. E. α-Hydroxynitrile Lyase in *Hevea brasiliensis* and its Significance for Rapid Cyanogenesis. *Physiol. Plant.* **1989**, *75*, 91–101.

(4) Kuroki, G. W.; Conn, E. E. Mandelonitrile Lyase from *Ximenia americana* L.: Stereospecificity and Lack of Flavin Prosthetic Group. *Proc. Natl. Acad. Sci. U.S.A.* **1989**, *86*, 6978–6981.

(5) Conn, E. E. *The Biochemistry of Plants: A Comprehensive Treatise*: Academic Press: New York, 1981, *7*; pp 479−500.

(6) Hickel, A.; Hasslacher, M.; Griengl, H. Hydroxynitrile Lyases: Functions and Properties. *Physiol. Plant.* **1996**, *98*, 891–898.

(7) Wajant, H.; Effenberger, F. Hydroxynitrile Lyases of Higher Plants. *Biol. Chem.* **1996**, *377*, 611–617.

(8) Lieberei, R.; Selmar, D.; Biehl, B. Metabolization of Cyanogenic Glucosides in *Hevea brasiliensis*. *Plant Syst. Evol.* **1985**, *150*, 49–63.

(9) Selmar, D. Apoplastic Occurrence of Cyanogenic Beta-Glucosidases and Consequences for the Metabolism of Cyanogenic Glucosides. *ACS Symp. Ser.* **1993**, *13*, 191–204.

(10) Effenberger, F. Synthesis and Reactions of Optically Active Cyanohydrins. *Angew. Chem., Int. Ed. Engl.* **1994**, *33*, 1555–1564.

(11) Griengl, H.; Hickel, A.; Johnson, D. V.; Kratky, C.; Schmidt, M.; Schwab, H. Enzymatic Cleavage and Formation of Cyanohydrins: a Reaction of Biological and Synthetic Relevance. *J. Chem. Soc., Chem. Commun.* **1997**, 1933–1940.

(12) Klempier, N.; Griengl, H.; Hayn, M. Aliphatic (*S*)-Cyanohydrins by Enzyme Catalyzed Synthesis. *Tetrahedron Lett.* **1993**, *34*, 4769–4772.

(13) Klempier, N.; Pichler, U.; Griengl, H. Synthesis of α/β-Unsaturated (*S*)-Cyanohydrins Using the Oxynitrilase from *Hevea brasiliensis*. *Tetrahedron: Asymmetry* **1995**, *6*, 845–848.

(14) Kruse, C. G. In *Chirality in Industry*; Collins, A. N., Sheldrake, G. N., Crosby, J., Eds.; John Wiley & Sons: New York, 1992; pp 279−299.

(15) Sharma, M.; Sharma, N. N.; Bhalla, T. C. Hydroxynitrile Lyase: At the Interface of Biology and Chemistry. *Enzyme Microb. Technol.* **2005**, *37*, 279–294.

(16) Khadjawi, M. G.; Parkarthofer, T.; Skranc, W.; Griengl, H. Hydroxynitrile Lyase-Catalyzed Enzymatic Nitroaldol (Henry) Reaction. *Adv. Synth. Catal.* **2007**, *349*, 1445–1450.

(17) Schmidt, A.; Gruber, K.; Kratky, C.; Lamzin, V. S. Atomic Resolution Crystal Structure and Quantum Chemistry Meet to Reveal Subtleties of Hydroxynitrile Lyase Catalysis. *J. Biol. Chem.* **2008**, *283*, 21827–21836.

(18) Gruber, K.; Gartler, G.; Krammer, B.; Schwab, H.; Kratky, C. Reaction Mechanism of Hydroxynitrile Lyases of the α/β-Hydrolase Superfamily. *J. Biol. Chem.* **2004**, *279*, 20501–20510.

(19) Wagner, U. G.; Hasslacher, M.; Griengl, H.; Schwab, H.; Kratky, C. Mechanism of Cyanogenesis: the Crystal Structure of Hydroxynitrile Lyase from *Hevea brasiliensis*. *Structure* **1996**, *4*, 811–822.

(20) Wajant, H.; Pfizenmaier, K. Identification of Potential Active-Site Residues in the Hydroxynitrile Lyase from *Manihot esculenta* by Site-Sirected Mutagenesis. *J. Biol. Chem.* **1996**, *271*, 25830–25834.

(21) Hasslacher, M.; Schall, M.; Hayn, M.; Griengl, H.; Kohlwein, S. D.; Schwab, H. Molecular Cloning of the Full-Length cDNA of (*S*)-Hydroxynitrile Lyase from *Hevea brasiliensis*. *J. Biol. Chem.* **1996**, *271*, 5884–5891.

(22) Hasslacher, M.; Schall, M.; Hayn, M.; Griengl, H.; Kohlwein, S. D.; Schwab, H. (*S*)-Hydroxynitrile Lyase from *Hevea brasiliensis*. *Ann. N. Y. Acad. Sci.* **1996a**, *799*, 707–712.

(23) Wajant, H.; Foerster, S. Purification and Characterization of Hydroxynitrile Lyase from *Hevea brasillensis*. *Plant Sci.* **1996**, *115*, 25–31.

(24) Wharton, C. W. The Serine Proteinases. In *Comprehensive Biological Catalysis*; Sinnott, M., Ed.; Academic Press: London, 1998.

(25) Zuegg, J.; Gruber, K.; Gugganig, M.; Wagner, U. G.; Kratky, C. Three-Dimensional Structures of Enzyme-Substrate Complexes of the Hydroxynitrile Lyase from *Hevea brasiliensis*. *Protein Sci.* **1999**, *8*, 1990–2000.

(26) Gruber, K. Elucidation of the Mode of Substrate Binding to Hydroxynitrile Lyase from *Hevea brasiliensis*. *Proteins: Struct., Funct., Genet.* **2001**, *44*, 26–31.

(27) Velichkova, P.; Himo, F. Methyl Transfer in Glycine *N*-Methyltransferase. A Theoretical Study. *J. Phys. Chem. B* **2005**, *109*, 8216–8219.

(28) Xie, D. Q.; Xu, D. G.; Zhang, L. D.; Guo, H. Theoretical Study of General Base-Catalyzed Hydrolysis of Aryl Esters and Implications for Enzymatic Reactions. *J. Phys. Chem. B* **2005**, *109*, 5259–5266.

(29) Georgieva, P.; Himo, F. Density Functional Theory Study of the Reaction Mechanism of the DNA Repairing Enzyme Alkylguanine Alkyltransferase. *Chem. Phys. Let.* **2008**, *463*, 214–218.

(30) Silva, P. J.; Ramos, M. J. Density-Functional Study of Mechanisms for the Cofactor-Free Decarboxylation Performed by Uroporphyrinogen III Decarboxylase. *J. Phys. Chem. B* **2005**, *109*, 18195–18200.

(31) Wang, J. Y.; Li, S. H. Catalytic Mechanism of 6-Phosphogluconate Dehydrogenase: A Theoretical Investigation. *J. Phys. Chem. B* **2006**, *110*, 7029–7035.

(32) Manojkumar, T. K.; Cui, C. Z.; Kim, K. S. Theoretical Insights into the Mechanism of Acetylcholinesterase-Catalyzed Acylation of Acetylcholine. *J. Comput. Chem.* **2005**, *26*, 606–611.

(33) Hopmann, K. H.; Himo, F. Theoretical Study of the Full Reaction Mechanism of Human Soluble Epoxide Hydrolase. *Chem.—Eur. J.* **2006**, *12*, 6898–6909.

(34) Fernandes, P. A.; Ramos, M. J. Theoretical Studies on the Mechanism of Inhibition of Ribonucleotide Reductase by (*E*)-2′-Fluoromethylene-2′-Deoxycitidine-5′-Diphosphate. *J. Am. Chem. Soc.* **2003**, *125*, 6311–6322.

(35) Wang, J.; Gu, J. D.; Leszczynski, J.; Feliks, M.; Sokalski, W. A. Oxime-Induced Reactivation of Sarin-Inhibited AChE: A Theoretical Mechanisms Study. *J. Phys. Chem. B* **2007**, *111*, 2404–2408.

(36) Beck, A. D. Density-Functional Thermochemistry. III. the Role of Exact Exchange. *J. Chem. Phys.* **1993**, *98*, 5648–5652.

(37) Lee, C.; Yang, W.; Parr, R. G. Development of the Colle-Salvetti Correlation-Energy Formula into a Functional of the Electron Density. *Phys. Rev. B* **1988**, *37*, 785–789.

(38) Miehlich, B.; Savin, A.; Stoll, H.; Preuss, H. Results Obtained with the Correlation Energy Density Functionals of Becke and Lee, Yang and Parr. *Chem. Phys. Lett.* **1989**, *157*, 200–206.

(39) Reed, A. E.; Weinstock, R. B.; Weinhold, F. Natural Population Analysis. *J. Chem. Phys.* **1985**, *83*, 735–746.

(40) Reed, A. E.; Weinhold, F. Natural Localized Molecular Orbitals. *J. Chem. Phys.* **1985**, *83*, 1736–1740.

(41) Reed, A. E.; Curtiss, L. A.; Weinhold, F. Intermolecular Interactions from a Natural Bond Orbital, Donor-Acceptor Viewpoint. *Chem. Rev.* **1988**, *88*, 899–926.

(42) Cancès, M. T.; Mennucci, B.; Tomasi, J. A New Integral Equation Formalism for the Polarizable Continuum Model: Theoretical Background and Applications to Isotropic and Anisotropic Dielectrics. *J. Chem. Phys.* **1997**, *107*, 3032–3041.

(43) Mennucci, B.; Tomasi, J. Continuum Solvation Models: A New Approach to the Problem of Solutes Charge Distribution and Cavity Boundaries. *J. Chem. Phys.* **1997**, *106*, 5151–5158.

(44) Cossi, M.; Barone, V.; Mennucci, B.; Tomasi, J. Ab initio Study of Solvated Molecules: A New Implementation of the Polarizable Continuum Model. *Chem. Phys. Lett.* **1996**, *255*, 327–335.

(45) Noodleman, L.; Lovell, T.; Han, W. G.; Li, J.; Himo, F. Quantum Chemical Studies of Intermediates and Reaction Pathways in Selected Enzymes and Catalytic Synthetic Systems. *Chem. Rev.* **2004**, *104*, 459–508.

(46) Zhao, Y.; García, N. G.; Truhlar, D. G. Benchmark Database of Barrier Heights for Heavy Atom Transfer, Nucleophilic Substitution, Association, and Unimolecular Reactions and Its Use to Test Theoretical Methods. *J. Phys. Chem. A* **2005**, *109*, 2012–2018.

(47) Selmar, R.; Lieberei, R.; Biehl, B.; Conn, E. E. α-Hydroxynitrile Lyase in *Hevea brasiliensis* and its Significance for Rapid Cyanogenesis. *Physiol. Plant.* **1989**, *75*, 97–101.

JP100373E